Z. Phys. A – Hadrons and Nuclei 344, 73–80 (1992)

Zeitschrift für Physik A Hadrons and Nuclei

Electromagnetic dissociation of relativistic heavy-ions in emulsion

G. Singh, P.L. Jain

Department of Physics, High Energy Experimental Laboratory, State University of New York at Buffalo, Buffalo, NY 14260, USA

Received: 5 March 1992 / Revised version: 27 May 1992

Abstract. We report the results on the electromagnetic dissociation of 14.5 A GeV ^{28}Si and 200 A GeV ^{16}O projectiles in nuclear emulsion. The overall charge changing production cross sections are determined experimentally and are found to agree reasonably well with those computed theoretically. The relative rate as a function of decay energy for various reaction channels are parameterized in terms of an exponential function. Majority of the events in the most prominent decay modes can be attributed to the excitation of giant dipole resonances. Multiplicity distributions of α particles emerged from nuclear as well as electromagnetic interactions are also investigated.

PACS: 25.70.Np; 25.20.−x

1. Introduction

During the last decade, beams of heavy ions have been accelerated at the BNL AGS and the CERN SPS to energies beyond those available at the LBL Bevalac, and consequently, these beams have been extensively employed as powerful tools to explore a variety of collision processes. Depending upon the value of the impact parameter, the collision between heavy-ions can give rise to two entirely different collision processes, viz., nuclear and electromagnetic. The former process is dominant, when a target and a projectile overlap even marginally. However, the latter process involves impact parameters larger than the range of nuclear force so that strong electromagnetic pulses are produced during a short period of time at the nucleus. Due to the Lorentz contraction, there is a considerable amount of enhancement in the strength of these pulses at relativistic energy. These strong electromagnetic pulses can lead to the excitation of nuclear giant dipole resonances (GDR) or to the creation of particles such as lepton pairs/pions, or to the excitation of new states with exotic decay modes [1]. For heavy targets, electromagnetic dissociation (ED) is expected to play an important role in the process of projectile fragmentation. First evidence for ED in relativistic heavy-ion collisions was reported in cosmic ray experiments [2, 3]. Later Heckman and Lindstrom [4] reported the evidence of ED of ^{12}C and ^{16}O projectiles at Bevalac energies, and subsequently, numerous experimental investigations have been performed on both projectile [5] and target [6] ED processes. Further information on this process has been obtained with different detectors exposed to ^{16}O, ^{32}S beams [7–9] at the CERN SPS and ^{28}Si ions [10–12] at the BNL AGS.

So far, very few experimental studies have been done on the ED using nuclear emulsion [13–15] exposed at the CERN SPS. At the BNL AGS, only one emulsion work exists on the ED of ^{28}Si ions [16], but with a much low statistics. In the present paper, we investigate the electromagnetic dissociation of the ^{28}Si beam from the AGS with a much better statistics than that given in [16]. We also compare the results obtained for the ED of ^{16}O beam at 200 A GeV from the CERN with the ^{28}Si projectile from the BNL.

Emulsion has the highest spatial resolution as compared to any other detector and it becomes extremely important especially at 200 A GeV energy, where the opening angles of the projectile fragments formed in ED events are very small ($\approx$1 mrad).

We shall briefly describe the classical theory of Weizsäcker and Williams [17] in Sect. II. In Sect. III, we give the experimental technique. Section IV is devoted to the results, which includes the charge spectra of the projectile fragments (PFs), mean free paths of nuclear (λ_{nuc}) and ED (λ_{ED}) events, relative rates of different decay modes, determination of the overall charge changing cross sections (σ_{ED}), the transverse momentum distributions (p_t) of protons in $\Delta Z = 1$ emission channel (as neutrons can not be detected in this experiment) and the comparison of multiplicity distribution of the α-fragments emerged in EDs and nuclear events. Finally, the conclusions of this work are given in Sect. IV.

2. Theory of electromagnetic dissociation

To explain the reaction mechanism involved in the electromagnetic collisions, the equivalent photon method was developed independently by Weizsäcker and Williams [17]. In this method, the projectile and the target are treated as point objects, and the number of photon quanta $N(E_\gamma)$ per unit area at an energy as seen by a moving projectile from the stationary target is given by

$$N(E_\gamma)=\frac{\alpha Z_T^2}{\pi\beta\gamma\hbar c E_\gamma}\left[x^2K_1^2(x)+(x^2/\gamma^2)K_0^2(x)\right], \quad (1)$$

where,

$$x=\frac{bE_\gamma}{\gamma\beta\hbar c}. \quad (2)$$

In (2), α is the fine structure constant, Z_T is the target charge, βc is the projectile velocity, γ is the Lorentz factor of the projectile in the laboratory frame and $K_1(K_0)$ are the modified Bessel functions of the order 1(0). The photon spectrum has an adiabatic cut off at an energy $E_\gamma^{\max}\approx\gamma\hbar c/b_{\min}$, where $b_{\min}=R_P+R_T$, the sum of the projectile and target radii. At AGS energies ($\approx$14.5 A GeV), $E_\gamma^{\max}\approx$300 MeV; whereas at CERN energies (200 A GeV), $E_\gamma^{\max}\approx$4 GeV. For photon energies $10<E_\gamma<40$ MeV, the most effective mechanism is through the exitation of giant dipole resonances. The quasideutron effect starts at energies $40<E_\gamma<140$ MeV, and for $E_\gamma>140$ MeV pion production takes place. The production of lepton pairs (e^+e^-, $\mu^+\mu^-$, $\tau^+\tau^-$) and the $\Delta(1232)$ resonances are accessible for higher values of energies.

For $\gamma\gg1$, (1) can be approximately written as

$$N(E_\gamma)=\frac{2Z_T^2\alpha}{\pi E_\gamma^{\max}}\left[\ln(1.123\,E_\gamma/E_\gamma^{\max})-1/2\right]. \quad (3)$$

A quantum mechanical approach using the plane wave Born approximation confirms the classical results, however, the photon spectra are distinct due to multipolarities [18].

The virtual photon spectra calculated on the basis of (3) are shown in Fig. 1a and b for the ^{28}Si at 14.5 A GeV and ^{16}O at 200 A GeV for different constituents of nuclear emulsion. The major contribution to ED in emulsion comes from Ag ($Z_T=47$) and Br ($Z_T=35$) nuclei, because the number of virtual photons varies as Z_T^2 (3). One can notice from Fig. 1 that the heaviest constituents of emulsion contribute more than 95% of the total photon intensity.

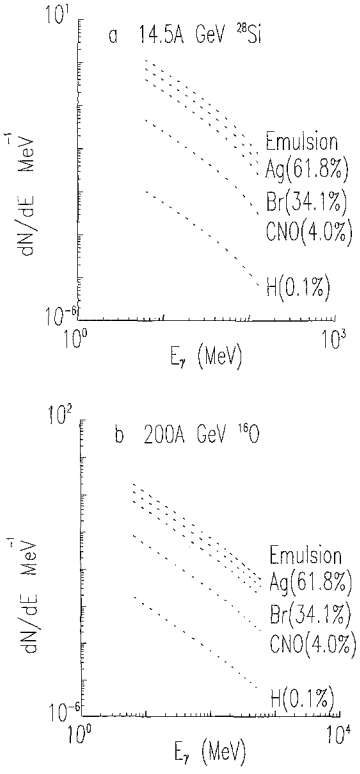

Fig. 1. The energy spectra of virtual photons for: **a** ^{28}Si beam at 14.5 A GeV and **b** ^{16}O beam at 200 A GeV in nuclear emulsion

3. Experimental technique

3.1. Exposure, scanning and selection of the events

The present study has been done in two emulsion stacks; one exposed to 14.5 GeV ^{28}Si ions at the BNL AGS (Exp. No. 847) and the other one to 200 A GeV ions at the CERN SPS (Exp. No. EMU08). The projectiles traversed the stacks parallel to the emulsion planes. To obtain high efficiency of scanning, the interactions of the beam particles were found using along-the-track scanning technique. The pellicles were scanned on digitized stage microscopes under 100$\times$ magnification. As the beams were very flat, the tracks were followed mostly in one pellicle. The primary tracks were picked up at a distance of 4 mm from the entrance edge of the pellicle and were carefully followed until they either interacted or escaped from the pellicle. In each interaction, the multiplicities of black tracks (N_b), grey tracks (N_g), the minimum ionizing shower tracks (n_s), singly charged projectile proton tracks (N_p) and the projectile fragments (PFs) of charge $Z\geqq2$ (N_f) were recorded. The charges of the PFs were determined by measuring the grain density, gap density, and by δ-ray counting as discussed in [13]. Each event was very carefully examined and qualitatively classified into three principal categories: *(i)* central, *(ii)* peripheral and *(iii)* electromagnetic events. A comprehensive discussion of the selection and classification of events is given elsewhere [13]. We followed track lengths of 174.89 m and 117.19 m corresponding to the beams 14.5 A GeV ^{28}Si and 200 A GeV ^{16}O and observed 1517 and 1070 interactions, respectively.

Since our analysis pertains to the EDs, it is very important to distinguish the nuclear peripheral events from the electromagnetic events. To achieve this necessary distinction, we impose a limit on the fragmentation cone for the PFs. The fragmentation cone is defined by $\Theta_{PF}\leqq\Theta_c=p_f/p_{\text{beam}}$, where, p_{beam} stands for the beam momentum and p_f for the Fermi momentum; the latter is estimated to be $\approx$160 MeV/c [19] for the ^{28}Si ions at

14.5 A GeV and thus giving $\Theta_c \approx 12$ mrad. For ^{16}O beam, the value of $\Theta_c \approx 1$ mrad [13]. The electromagnetic events were picked up among the peripheral ones with no visible excitation of the target nucleus (N_g and $N_b = 0$) and with an additional constraint that the sum of charges of all the PFs with $Z \geqq 1$ inside the fragmentation cone is always 14 for the ^{28}Si beam. The contribution of the nuclear peripheral events in our samples of the electromagnetic events is effectively minimized subject to the requirement that the number of produced shower particles (n_s) in ED events $\leqq 1$. Exclusion of low energy e^+e^- pairs, high energy δ-rays and the elastic scattering events was done as discussed in [13]. For 200 A GeV ^{16}O beam, the EDs have been identified by adopting exactly the same selection criteria as given in [13]. By applying these stringent selection criteria, the numbers of EDs corresponding to the beams ^{28}Si and ^{16}O were 109 and 113, respectively. For ^{28}Si beam, all 109 electromagnetic events were found to be due to the clean breakup of the projectile and with no visible excitation of the target nucleus (N_b and $N_g = 0$). However, for the ^{16}O sample of ED events, 8 events had a single pion track and the remaining 105 events were due to the clean breakup of the ^{16}O projectile.

3.2. *Space angle measurements of* PFs *in* ED *events*

The space angles of the projectiles fragments in EDs, were determined from the vector directions of the emitted tracks with respect to a non-interacting primary track (the reference primary track) selected in the vinicity of the interaction vertex. The x-, y- and z-coordinates of all the PFs including the vertex and reference primary track were subjected to three dimensional track reconstruction programs, which computed the space angles. This technique gives an accuracy better than 0.1 mrad for the angles $\theta \leqq 1$ mrad, including the error due to the multiple Coulomb scattering [20].

4. Results

4.1. *The charge spectra*

In Fig. 2a, we show the charge spectrum of all the PFs ranging from $Z = 1$ to $Z = 13$ for the ^{28}Si beam, while a similar plot for the PFs with charges $Z = 1$–7 emitted in the ^{16}O beam is shown in Fig. 2b. In both of these Fig., the most abundant PF is with $Z = 1$, the next one is with $Z = 2$. The least abundant are the charges in the range of $3 \leqq Z \leqq 5$ for both of the beams. For heavier ^{28}Si beam, there is a slow increase in the relative abundances of charges between $6 \leqq Z \leqq 11$. Charge $Z = 13$ has the relative yield almost two times than that of $Z = 12$ and this conclusion is also valid for the PFs of charges $Z = 7$ and $Z = 6$ in the case of ^{16}O beam.

4.2. *Nuclear* (λ_{nuc}) *and* ED (λ_{ED}) *mean free paths*

In Table 1, we present the topologies of the inelastic and electromagnetic interactions observed. We also include here the results from [15] and [16] on different types of

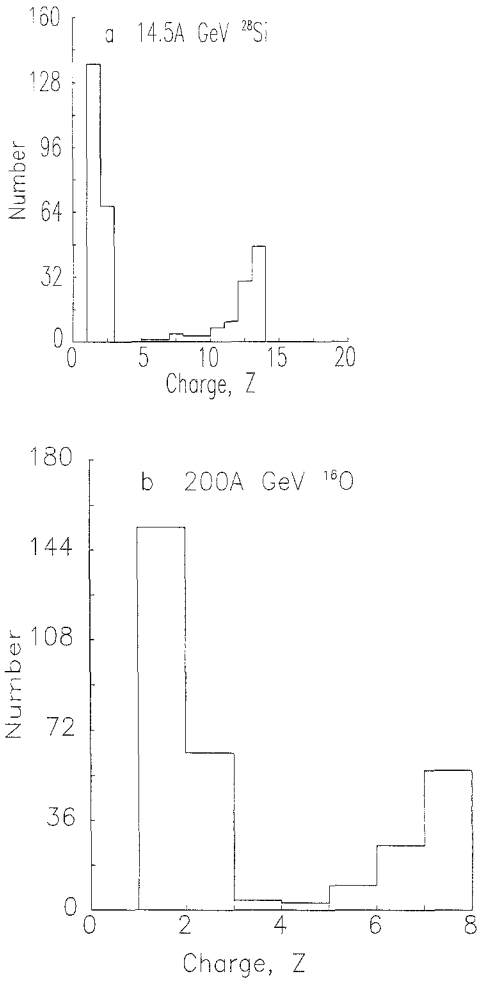

Fig. 2. a Charge spectrum of the PFs with $1 \leqq Z \leqq 13$ for ^{28}Si at 14.5 A GeV. **b** The same as a, but for PFs of charges $1 \leqq Z \leqq 7$ for ^{16}O at 200 A GeV

interactions. Table 1 indicates that ED as a percentage of the nuclear events (N_{nuc}) increases with the total projectile energy. For projectiles having almost the same masses and different energies (^{32}S at 200 A GeV and ^{28}Si at 14.5 A GeV), the value of λ_{ED} decreases as the projectile energy is increased from 14.5 A GeV to 200 A GeV. For ions having the same energy per nucleon but of different masses (^{32}S and ^{16}O at 200 A GeV), heavier projectile has less value of λ_{ED}. These observations are in qualitative agreement with the predictions of the virtual photon theory [7, 8, 17, 18]. From λ_{nuc}, one can calculate the nuclear cross sections, which is discussed in Sect. 4.4.

4.3. *Observed modes of decay in* ED

In Table 2a and b, we present a summary of the identified ED events in ^{28}Si and ^{16}O – emulsion collisions, respectively. Results from the [7], [10], [15] and [16] are also included to facilitate the comparison. In the first column of these Tables, the decay mode of an observed channel, deduced from the charge conservation, is given. The second column shows the threshold energy (ΔE_{th}) for the excitation of a given mode calculated in the rest frame

Table 1. The data on the number of primary nuclear (N_{nuc}) and electromagnetic dissociated (N_{ED}) interactions of different ions in nuclear emulsion

Ion	Energy (A GeV)	Length followed (m)	N_{nuc}	N_{ED}	λ_{nuc} (cm)	λ_{ED} (cm)	ED as % of N_{nuc}	Ref.
^{28}Si	14.5	174.89	1408	109	12.42 ± 0.33	160.45 ± 15.37	7.74	This work
^{28}Si	14.6	71.69	691	46	10.37 ± 0.39	155.85 ± 22.98	6.66	[16]
^{16}O	200	117.19	957	113	12.25 ± 0.40	103.71 ± 9.76	11.81	This work
^{16}O	200	69.31	591	68	11.73 ± 0.48	101.91 ± 12.36	11.11	[16]
^{16}O	200	348.70	2934	362	11.88 ± 0.22	96.33 ± 5.10	12.34	[15]
^{32}S	200	198.50	2168	476	9.15 ± 0.20	41.70 ± 1.91	2196	[15]

Table 2a. In different decay modes for ^{28}Si at 14.5 A GeV, threshold energy (ΔE_{th}), observed number of EDs (N_{ED}) and ED fractions are presented

Decay mode	Threshold energy (MeV)	N_{ED}	Fraction (%)		
			Present work	[16]	[10]
^{27}Al$+p$	11.6	47	43.12 ± 6.29	32.61 ± 8.42	67.32 ± 19.38
^{24}Mg$+2d$	48.7	13	27.52 ± 5.02	30.43 ± 8.13	16.73 ± 4.82
^{24}Mg$+\alpha$	10.0	17			
^{23}Na$+\alpha+p$	21.7	10	9.17 ± 2.90	8.70 ± 4.35	2.33 ± 0.67
^{20}Ne$+2\alpha$	19.8	2	6.42 ± 2.43	8.70 ± 4.35	1.17 ± 0.34
^{20}Ne$+\alpha+2d$	43.2	4			
^{20}Ne$+4d$	70.02	1			
^{19}F$+2\alpha+p$	26.8	1	2.75 ± 1.59	–	1.17 ± 0.34
^{19}F$+\alpha+2d+p$	56.0	2			
^{16}O$+2\alpha+2d$	47.9	2	2.75 ± 1.59	6.52 ± 3.77	1.56 ± 0.45
^{16}O$+\alpha+4d$	71.8	1			
^{14}N$+3\alpha+d$	47.9	2	3.67 ± 1.83	4.35 ± 3.07	1.17 ± 0.34
^{14}N$+2\alpha+3d$	68.6	2			
^{12}C$+\alpha+6d$	102.8	1	4.59 ± 2.05	–	8.56 ± 1.75 ($Z \leq 6$)
^{11}B$+3\alpha+2d+p$	71.0	1			
$6\alpha+2d$	62.3	1			
$5\alpha+4d$	86.2	1			
$3\alpha+8d$	133.9	1			

Table 2b. Same as **a**, but for ^{16}O beam at 200 A GeV

Decay mode	Threshold energy (MeV)	N_{ED}	Fraction (%)			
			Present work	[16]	[15]	[7]
^{15}N$+p$	11.1	54	49.45 ± 6.62	38.24 ± 7.50	56.08 ± 3.93	55.00 ± 3.00
^{12}C$+\alpha$	7.2	10	23.01 ± 4.80	26.47 ± 7.70	25.58 ± 2.61	17.00 ± 2.00
^{12}C$+2d$	31.0	13				
^{11}B$+\alpha+p$	23.1	6	10.62 ± 3.06	8.82 ± 3.60	4.42 ± 1.10	28.00 ± 6.00 ($Z \leq 5$)
^{8}Be$+\alpha+2d$	47.0	3				
^{8}Be$+^{7}$Li$+p$	32.4	1				
^{7}Li$+2\alpha+p$	31.8	2	4.42 ± 1.98	4.41 ± 2.55	2.49 ± 0.83	–
^{7}Li$+\alpha+2d+p$	55.6	2				
^{7}Li$+4d+p$	79.5	1				
4α	14.4	4	12.39 ± 3.31	14.71 ± 4.65	8.01 ± 1.49	–
$3\alpha+2d$	38.3	4				
$2\alpha+4d$	62.1	4				
$\alpha+6d$	86.0	1				
^{15}N$+p+\pi$	>200	2				
^{12}C$+2d+\pi$	>200	3				
^{11}B$+3d+\pi$	>200	1				
^{8}Be$+\alpha+2d+\pi$	>200	1				
$3\alpha+2d+\pi$	>200	1				

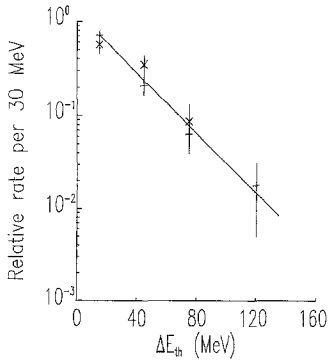

Fig. 3. Variation of the relative rate per 30 MeV as a function of threshold energy ΔE_{th} for different decay modes in EDs. Symbols used are: *(i)* this work (+) and *(ii)* Bahk et al. (×). Solid line is a least squares fit to the data points

of the projectile by using the mass defect formula [21]. The third column indicates the number of ED events (N_{ED}) observed in each mode. The fourth column gives the relative rates for the various visible modes. To calculate the percentile abundances of various decay modes for [10], we have taken the values of the σ_{ED} for Ag and Cu targets, since in emulsion experiment, the heavier targets Ag and Br contribute almost 96% to the observed ED cross section. The relative rates, within the statistical errors, are close to those of [16] for the ^{28}Si data. A similar conclusion is also true for the 200 A GeV ^{16}O data of present study and of [7], [15] and [16] [Table 2b]. However, there are some discrepancies between our data and of [7] for ^{28}Si projectile at 14.5 A GeV. These discrepancies may be due to low statistics of both the data samples or due to different detection techniques used here and in [7]. We may point out that in this study 18 and 14 decay modes have been observed for ^{28}Si and 200 A GeV ^{16}O projectiles, respectively. In Fig. 3 is shown the relative rate (per 30 MeV) of different decay modes as a function of the threshold energy (ΔE_{th}) in ED events from ^{28}Si beam. Data of Bahk et al. for ^{28}Si beam are also included in this figure. These data can be approximately represented by the relation $Y=\exp(k_1 \Delta E_{th}+k_2)$, where, $k_1=-0.036\pm0.011$ MeV^{-1} and $k_2=0.022$, with $\chi^2/\mathrm{DOF}=0.02$. Here, DOF stands for the degrees of freedom. The value of k_1 determined in this work is close to that in [16].

4.4. Cross sections σ_{nuc} and σ_{ED}

In Table 3, we display our experimental data along with the data of other investigators on the production cross sections for nuclear [15, 16] and electromagnetic events [7, 8, 10, 15, 16]. The cross section is calculated from the relation $\sigma=f/\rho\lambda$, where, $\rho=7.898\times10^{22}$ atoms per cm^3 [22] and f is a weight factor which is unity for nuclear interactions produced by all the emulsion targets. To compare experimental values of nuclear cross sections σ_{nuc} with a theoretical prediction, the semiempirical expression for the geometrical cross section σ_{nuc}^{th} of [13] has been employed for projectiles and targets of mass $A_P \geqq 12$

Table 3. Nuclear cross section (σ_{nuc}) for all targets of emulsion and ED cross section (σ_{ED}) for the Ag target only. The weight factor f is explained in the text

Beam	Energy (A GeV)	σ_{nuc}(mb)	f	σ_{ED}(mb)	Ref.
^{28}Si	14.5	1019 ± 27	0.62	383 ± 37	This work
	14.5	1221 ± 46	0.62	394 ± 58	[16]
	14.5	-	-	300 ± 100	[10]
^{16}O	200	1033 ± 38	0.62	592 ± 57	This work
	200	1079 ± 44	0.62	602 ± 73	[16]
	200	1066 ± 20	0.61	670 ± 35	[15]
	200	-	-	652 ± 59	[7]
^{32}S	200	1384 ± 30	0.61	1680 ± 80	[15]
	200	-	-	1790 ± 120	[8]

and $A_T \geqq 12$. As discussed in [9] for the validity of the usage of expression given in [13] for hydrogen target, we have chosen $A_T=0.089$. Using this value of A_T for hydrogen target and the other ones of heavier targets of nuclear emulsion, in conjunction with their number densities [22], theoretical values of nuclear cross sections σ_{nuc}^{th} are 1460 mb, 1392 mb and 1152 mb, for ^{32}S, ^{28}Si and ^{16}O projectiles, respectively. The calculated value of σ_{nuc}^{th} for ^{16}O at 200 A GeV agrees quite well with those of measured ones (σ_{nuc}) within the experimental errors (Table 3). For ^{32}S at 200 A GeV and ^{28}Si at 14.5 A GeV, theory gives a little higher values of σ_{nuc}^{th}, when we compare these results with those obtained experimentally. To explain these results for ^{32}S at 200 A GeV and ^{28}Si at 14.5 A GeV, theory needs some modifications. In order to obtain the absolute value of the cross section for EDs and also to compare the present results with other experiments, we converted the observed mean free path in emulsion into absolute cross section on Ag target (the heaviest and most abundant element in emulsion). The contribution of the elements such as iodine and sulphur, whose abundances in nuclear emulsion are very small, is neglected. The total production cross section for ED events on the Ag target is then computed from the above relation by substituting the value of λ for the ED events and $\rho=1.01\times10^{22}$ atoms per cm^3 - the density of Ag target in standard nuclear emulsion [22]. The factor f is an appropriate weightage obtained for the Ag targets from the following equation: $f=N_T Z_T^2/\Sigma N_i Z_i^2$, where N_T is the number of Ag atoms/ml in standard nuclear emulsion and $Z_T=47$, is its nuclear charge. Denominator represents a summation over all the targets (viz., Ag, Br, C, N, O, and H) of nuclear emulsion [22]. The value of f obtained in the present work is 0.62. The values of σ_{ED}, thus obtained, are given in Table 3. In order to determine σ_{ED} for the data of [16], the weight factor of the present investigation has been employed, while for the data of [15], the weight factor given in that reference is used. Table 3 also includes the data collected with plastic foil detectors taken from [10], [7] and [8] for the ^{28}Si, ^{16}O and ^{32}S beams, respectively. In spite of the fact that σ_{ED} obtained in the present work and in other experiments [7], [8] and [10] have employed completely different detection techniques, the overall agreement of the ED cross sections is reasonably good. This shows that a he-

trogeneous emulsion detector can also be employed successfully to measure the ED cross sections at relativistic energies. When we compare our measured values of the production cross sections (Table 3) with those computed theoretically in [10] and [7] for ^{28}Si and ^{16}O projectiles, respectively, the agreement between the experiment and theory seems to be quite good.

5. Transverse momentum distribution of protons

In our experiment, it is possible to determine the transverse momentum (p_t) of protons, released in the most prominent decay modes (Tables 2), from the measured values of the space angles (θ), and consequently, the decay energy (ΔE_d) can be determined for the excitation of a resonant state. The decay energy, in fact, is the energy transferred to the relativistic projectile (P) from a stationary target (T) in ED process. According to the WW theory [17], the transverse momentum imparted to the projectile nucleus is given by

$$p_t = \frac{2 Z_P Z_T e^2}{v b_{\min}}, \tag{4}$$

where, eZ_P and eZ_T are the charges of the projectile and target, respectively, $v \approx c$ is the projectile velocity and $b_{\min} = 1.35 (A_P^{1/3} + A_T^{1/3})$ fm [13], where A_P and A_T are the mass numbers of the projectile and target nuclei, respectively. In Fig. 4a and b, we draw the p_t distributions of protons produced in the reactions $^{28}\text{Si} \rightarrow {}^{27}\text{Al} + p$ and $^{16}\text{O} \rightarrow {}^{15}\text{N} + p$, respectively. The p_t values are calculated with the assumption that the projectile protons have the same longitudinal momenta as that of the incident beam particles. In distributions shown in Fig. 4a and b, the peak values of p_t correspond to $\approx 170 \pm 25$ MeV/c and $\approx 180 \pm 24$ MeV/c, respectively, for the ^{28}Si (γ, p) ^{27}Al and $^{16}\text{O}(\gamma, p)$ ^{15}N decay modes. Using (4), the calculated values of p_t for the above decay modes are ≈ 140 and 160 MeV/c, showing that experimental values within the errors are in close agreement to the theoretical ones. Price and He [19] determined p_t value for the PFs emitted in nuclear interactions for the ^{28}Si beam at 14.5 A GeV and obtained $p_t \approx 160$ MeV/c, which agrees favourably with our experimental value ($\approx 170 \pm 25$ MeV/c). Transverse momentum p_t of a resonant state for the decay mode $A' \rightarrow B' + C'$ is $p_t = \sqrt{2 m_0 \Delta E_d}$, where ΔE_d is the decay energy of a resonant state and m_0 is the reduced mass of $B' + C'$. From the measured values of p_t, the decay energies determined for the modes $^{28}\text{Si} \rightarrow {}^{27}\text{Al} + p$ and $^{16}\text{O} \rightarrow {}^{15}\text{N} + p$ are, $\Delta E_d \approx 16 \pm 2$ MeV and 17 ± 2 MeV, respectively. By comparing these values of decay energies with those of threshold energies (ΔE_{th}) given in Table 2, one can notice that the measured values of ΔE_d are well above the excitation of the respective resonant states for the emission of a nucleon in the reaction $A' \rightarrow B' + C'$. Former studies on nuclei of mass numbers $A > 130$ have shown that the giant dipole resonance is located approximately [18] at $E_{\text{GR}}^{(1)} = 80/A_P^{1/3}$. However, for lighter nuclei the resonance energy falls off steadily from the value given by this equation [23]. In case of ED events induced

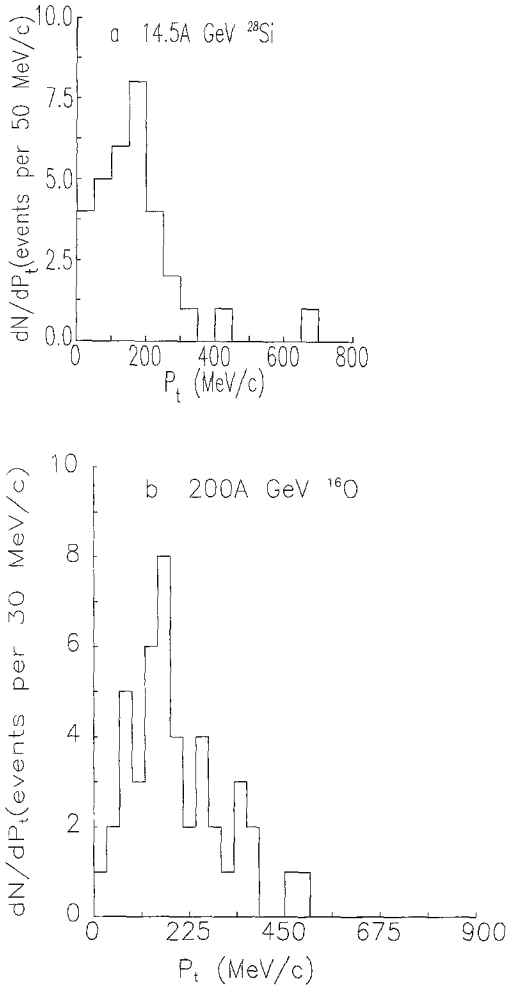

Fig. 4. Transverse momentum (p_t) distributions of protons in: **a** $^{28}\text{Si}(\gamma, p)$ ^{27}Al and **b** $^{16}\text{O}(\gamma, p)$ ^{15}N decay modes

by ^{28}Si at 14.5 A GeV, from the above equation, we have $E_{GR}^{(1)} \approx 26$ MeV. Recently, Alarcon et al. [24] have measured the total photoabsorption cross section σ_γ using photons of incident energies in the range $17 \leqq E_\gamma \leqq 28$ MeV by the scattering measurements of quasi-monochromatic photons impinging on the ^{28}Si target. The giant dipole resonances in their experiments were observed in the range $16 < E_\gamma < 24$ MeV. From these arguments, a great majority of events in the decay reaction $^{28}\text{Si} \rightarrow {}^{27}\text{Al} + p$ may be explained due to the absorption of giant dipole resonances and similar arguments may also be given to explain the decay mode $^{16}\text{O} \rightarrow {}^{15}\text{N} + p$. Because of the low statistics, it was not possible for us to extend this analysis to the other prominent decay modes. In a very recent study on the reaction channel $^{28}\text{Si}(\gamma, p)$ ^{27}Al, Barrette et al. [12] also find the occurence of giant dipole resonances in the expected region for ^{28}Si ions at 14.6 A GeV with a much bigger statistics.

6. Multiplicity distributions of α fragments

Finally, we study the multiplicity distributions of the α fragments produced in nuclear and ED interactions, since such a study is quite important in understanding the re-

action mechanism involved. As predicted by Koba et al. [25], multiplicity distributions $P(n)$ in relativistic collisions obey a scaling law:

$$\psi(z) = \langle n_\alpha \rangle P(n_\alpha) = \langle n_\alpha \rangle \sigma_{n\alpha}/\sigma_{\text{nuc}}, \quad (5)$$

which is an energy independent function of the scaled variable $z = n_\alpha/\langle n_\alpha \rangle$, where n_α represents the number of α particles produced in an event and $\langle n_\alpha \rangle$ is the average α multiplicity of the whole data sample. In (5), σ_{nuc} refers to the total nuclear cross section and $\sigma_{n\alpha}$ is the partial cross section for producing a state of multiplicity n_α. For the first time, we showed in [26] the onset of α fragment scaling and later on in [27]. It was shown that the multiplicity distributions of the produced α fragments from the events of different projectiles over a wide range of energies can be represented by a universal function of the following form:

$$\psi(z) = Az\exp(-Bz), \quad (6)$$

where A and B are constants, whose values are given in [26]. In Fig. 5a, we plot $\langle n_\alpha \rangle P(n_\alpha)$ as a function of the scaled variable $n_\alpha/\langle n_\alpha \rangle$ for the α fragments emerged in EDs, whereas a similar distribution is shown in Fig. 5b for the nuclear events. The following functional form has been fitted through the data points of Fig. 5a: $\psi(z) = az^b$, where, $a = 0.28$ and $b = -1.24$, with $\chi^2/\text{DOF} = 0.38$. However, the multiplicity distributions of the α fragments emerged in nuclear events, viz. Fig. 5b, for different projectiles lie on a simple universal curve represented by (6). The values of the constants are $A = 4.65$ and $B = 2.10$ with $\chi^2/\text{DOF} = 0.03$. The fact that two different functional forms must be fitted through the data points for EDs and nuclear events, may be a consequence of their different reaction mechanism involved.

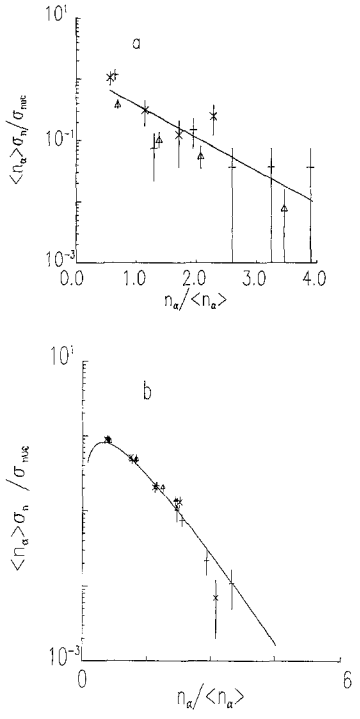

Fig. 5. The multiplicity distribution of $\langle n_\alpha \rangle \sigma_{n\alpha}/\sigma_{\text{nuc}}$ as a function of the scaled variable $n_\alpha/\langle n_\alpha \rangle$ of the α fragments for: **a** EDs and **b** nuclear events. Symbols used in these figures are for: *(i)* ^{28}Si at 14.5 A GeV (+), *(ii)* ^{16}O at 200 A GeV (×), *(iii)* ^{32}S at 200 A GeV (△) and *(iv)* for ^{16}O at 60 A GeV (▲). Solid curves represent the theoretical fitting of the data as explained in text

7. Conclusions

In this paper, we have investigated the ED of 14.5 A GeV ^{28}Si from the AGS and 200 A GeV ^{16}O ions from the CERN SPS. The results are compared with available data on electromagnetic interactions. The following are the important conclusions of this work:

at BNL energies, the electromagnetic dissociation of ^{28}Si projectile represents $\approx 8\%$ of the total number of nuclear events observed, while at the CERN energies, we find this number as $\approx 12\%$ for the 200 A GeV ^{16}O beam. The above values agree quite well with those given in [16] and [15] for the ^{28}Si and ^{16}O data. A similar conclusion is also valid for the relative rates of the visible decay modes for these projectiles.

The absolute values of the overall charge changing cross sections (σ_{ED}) for the Ag target are determined experimentally. Within statistical errors, our results are very close to the observations of other investigators (Table 3). The value of σ_{ED} increases as a function of the total incident energy for the ions used in this experiment. The overall charge changing cross sections agree quite well with the theory.

The excitations energies as determined from the measured values of p_t for the projectile protons in decay modes $^{28}\text{Si} \rightarrow {}^{27}\text{Al} + p$ and $^{16}\text{O} \rightarrow {}^{15}\text{N} + p$ are well above the threshold energies for the formation of respective resonant states. Majority of the events in these modes may be attributed to the absorption of giant dipole resonances.

The multiplicity distributions of the α fragments in EDs and nuclear events have been fitted through different functional forms. This difference may be a consequence of the different reaction mechanisms involved in EDs and nuclear events.

We are thankful to Dr. D. Beavis, BNL for his help in exposure and to Prof. G. Romano, CERN for the development of our emulsion stack and to Mr. Tetsuo Kurokawa for the scanning work. This work was supported by the Grant No. DE-FGO2-90ER40566.

References

1. Munzinger, P.B.: In: Response of nuclei under extreme conditions. Broglia, R.A., Bertsch, G.E. (eds.). New York: Plenum Press 1988
2. Rybicki, K.: Nuovo Cimento **49**, 203 (1967); Balasubramanyan, V.K.: Proceedings of the 12th Int. Conf. on Cosmic Rays, Hobart, Tasmania 1972
3. Artu, X., Yodh, G.B.: Phys. Lett. B**40**, 43 (1972)
4. Heckman, H.H., Lindstrom, P.J.: Rev. Lett. **37**, 56 (1976)
5. Olsen, D.L., Berman, B.L., Greiner, D.E., Heckman, H.H., Lindstrom, P.J., Westfall, G.D., Crawford, H.J.: Phys. Rev. C**24**, 1529 (1981); Westfall, G.D., Wilson, L.W., Lindstrom,

P.J., Crawford, H.J., Greiner, D.E., Heckman, H.H.: Phys. Rev. C**19**, 1309 (1979)
6. Hill, H.J., Wohn, F.K., Winger, J.A., Smith, A.R.: Phys. Rev. Lett. **60**, 999 (1988); Mercier, M.T., Hill, J.C., Wohn, F.K., McCullough, C.M., Nieland, M.E., Winger, J.A., Howard, C.B., Renwick, S., Methesis, D.K., Smith, A.R.: Phys. Rev. C**33**, 1655 (1986)
7. Brechtmann, C., Heinrich, W.: Z. Phys. A - Atomic Nuclei **330**, 407 (1988)
8. Brechtmann, C., Heinrich, W.: Z. Phys. A - Atomic Nuclei **331**, 463 (1988)
9. Price, P.B., Guoxia, R., Williams, W.T.: Phys. Rev. Lett. **61**, 2193 (1988)
10. Brechtmann, C., Heinrich, W., Benton, E.V.: Phys. Rev. C**39**, 2222 (1989)
11. Llope, W.J., Braun-Munzinger, P.: Phys. Rev. C**41**, 2644 (1990)
12. Barrette, J., Braun-Munzinger, P., Cleland, W.E., David, G., Duck, E., Fatyga, M., Fox, D., Greene, S.V., Hall, J.R., Heifetz, R., Hemmick, T.K., Herrmann, N., Hogue, R.W., Ingold, G., Jayananda, K., Kraus, D., Legault, A., Lissauer, D., Llope, W.J., Ludlam, T., Majka, R., Makowiecki, D., Mark, S.K., Mitchell, J.T., Muthuswamy, M., O'Brien, E., Olsen, L.H., Polychronakos, V., Rawool-Sullivan, M., Rotondo, F.S., Sandweiss, J., ShivaKumar, B., Simon, J., Sonnandara, U., Stachel, J., Sunier, J., Takai, H., Throwe, T.G., Vanhecke, H., Waters, L., Willis, W.J., Wolfe, K., Woody, C.L.: Phys. Rev. C**41**, 1512 (1990); Barrette, J., Bellwied, R., Braun-Munzinger, P., Cleland, W.E., David, G., Dee, J., Dietzsch, O., Duek, E., Fatyga, M., Fox, D., Greene, S.V., Hall, J.R., Hemmick, T.K., Herrmann, N., Hogue, R.W., Hong, B., Jayananda, K., Kraus, D., ShivaKumar, B., Lacasse, R., Lissauer, D., Llope, W.J., Ludlam, T., Majka, R., Makowiecki, D., Mark, S.K., McCorkle, S., Mitchell, J.T., Muthuswamy, M., O'Brien, E., Polychronakos, V., Pruneau, C., Rotondo, F.S, Sandweiss, J., Simon-Gillo, J., Sonnandara, U., Stachel, J., Takai, H., Takagui, E.M., Throwe, T.G., Waters, L., Willis, W.J., Winter, C., Wolf, K., Wolfe, D., Woody, C.L., Xu, N., Zhang, Y., Zou, Z.: Phys. Rev. C**45**, 2427 (1992)
13. Singh, G., Sengupta, K., Jain, P.L.: Phys. Rev. C**41**, 999 (1990)
14. Ardito, N., Baroni, G., Bisi, V., Breslin, A.C., Davis, D.H., Dell'Uomo, S., DiLiberto, S., Guibellino, P., Hoshino, K., Kodama, K., Marzari-Chiesa, A., Masera, M., Mazzoni, M.A., Meddi, F., Montwill, A., Muciaccia, M.T., Natali, S., Niu, K., Niwa, K., Poulard, G., Ramello, L., Riccati, L., Romano, G., Rosa, G., Sgarbi, C., Simone, S., Sletten, H., Tovee, D.N., Vanderhaeghe, G.R., Wilkin, C.: Europhys. Lett. **6**, 131 (1988)
15. Baroni, G., Bisi, V., Breslin, A.C., Davis, D.H., Dell'Uomo, S., Di Liberto, S., Guibellino, P., Grella, G., Hoshino, K., Kazuno, M., Kobayashi, M., Kodama, K., Marzari-Chiesa, A., Mazzoni, M.A., Meddi, F., Muciaccia, M.T., Niu, K., Ramello, L., Romano, G., Rosa, G., Sgarbi, C., Shibuya, H., Simone, S., Tovee, D.N., Ushida, N., Wilkin, C., Yuen, S.K.C.: Nucl. Phys. A**516**, 673 (1991)
16. Bahk, S.Y., Chang, S.D., Cheon, B.G., Cho, J.H., Jang, H.I., Hahn, C.H., Hara, T., Lim, G.Y., Kang, J.S., Kim, C.O., Kim, J.Y., Kim, K.Y., Kim, S.N., Kim, T.I., Kim, T.Y., Koo, D.G., Lee, S.B., Lim, I.T., Moon, K.H., Nam, S.W., Pac, M.Y., Park, I.G., Park, J.N., Ryu, J.Y., Shin, T.S., Sim, K.S., Song, J.S., Woo, J.K., Yokoyama, C., Yoon, C.S.: Phys. Rev. C**43**, 1410 (1991)
17. Jackson, J.D.: Classical electrodynamics. 2nd ed. Chap. 15, p. 619. New York: Wiley 1975
18. Bertulani, C.A., Baur, G.: Nucl. Phys. A**442**, 739 (1985)
19. Price, P.B., He, Y.D.: Phys. Rev. C**43**, 835 (1991)
20. Jain, P.L., Sengupta, K., Singh, G.: Phys. Rev. C**44**, 844 (1991)
21. Kaplan, I.: Nuclear physics, 2nd ed., Chap. 9, p. 221. Reading, Mass.: Benjamin 1962
22. Barkas, W.H.: Nuclear research emulsion, p. 73. New York: Academic Press 1963
23. Bertrand, F.E.: Nucl. Phys. A**354**, 129c (1981)
24. Alarcon, R., Nathan, A.M., LeBrun, S.F., Hoblit, S.D.: Phys. Rev. C**39**, 324 (1989)
25. Koba, Z., Nielsen, B., Olesen, P.: Nucl. Phys. B**40**, 317 (1972)
26. Jain, P.L., Aggarwal, M.M.: Phys. Rev. C**33**, 1790 (1986)
27. Singh, G., Ismail, A.Z.M., Jain, P.L.: Phys. Rev. C**43**, 2417 (1991)